modify the relation of Figures 3 and 4, or the effect of the Baldwin effect in the abundance determination as Sameshima et al. (2020) have tested for Fe II/Mg II. Enlarging the sample is one of the main challenges. For observing the CaT in sources with $z > 2$, NIR spectrometers with higher sensitivity are required. However, due to the fact that the NIR and mid-IR spectral regions are strongly affected by atmospheric telluric bands, some redshift ranges will remain inaccessible from ground-based telescopes The most attractive possibility to study the Fe II/CaT ratio at larger redshifts is offered by upcoming space observatories, such as the Near InfraRed Spectrograph (NIRSpec) from the James Webb Space Telescope (JWST).

7. Conclusions

We performed a detailed analysis of the observational correlations present in our CaT-Fe II sample, together with a bootstrap analysis to assess the statistical reliability of the correlations. Throughout a PCA, we identify the primary driver of our sample. We could not find any redshift dependence above the 2σ confidence level. Since our sample is flux limited, the presented analysis must be confirmed by larger samples in the future. The presented analysis shows the following:

1. The correlations with luminosity, black hole mass, and Eddington ratio are stronger for CaT than for Fe II. This suggests that CaT is a better proxy for the Eddington ratio than Fe II. A potential application of this result could be, for example, the correction of the RL relation for effects dependent on the accretion rate. However, the bootstrap analysis provides a probability of 50% of detecting a false-positive relation. Therefore, a more complete sample is needed to confirm this result.
2. The $EW_{H\beta}$ correlates negatively with luminosity (Baldwin effect), while the EW_{CaT} shows a positive correlation. This stresses the different nature of both low-ionization emission lines. In general, the correlations with Eddington ratio are stronger, are more reliable, and show the smallest errors according to the bootstrap analysis. This supports the Eddington ratio as the driver of the Baldwin effect.
3. We performed a PCA to deduce the driver for the R_{CaT}–R_{FeII} relation observed in our sample. We confirm that the results of the PCA are dependent on the selection of the sample and the chosen quantities. We consider only the directly observable variables (FWHMs, luminosity, and EWs) in the final PCA and later correlate the first four eigenvectors to the derived variables (bolometric luminosity, black hole mass, Eddington ratio, the ratios—R_{FeII} and R_{CaT}, and the metallicity indicator, Fe II/CaT). The dominant eigenvector is primarily driven by the combination of black hole mass and luminosity, which in turn is reflected in the strong correlation of the first eigenvector with the Eddington ratio. We also notice a noticeable correlation of the primary eigenvector with the metallicity tracer, Fe II/CaT.
4. Combining the PCA results and the observational correlation, we conclude that luminosity, black hole mass, and Eddington ratio are the main drivers of our sample; however, the correlations are better described by the Eddington ratio, setting this parameter one step ahead in comparison to the other parameters. A larger, more complete sample spanning a larger redshift range including a wide variety of AGNs is needed to assert the driver(s) of the CaT−Fe II correlations.
5. We found a significant negative increment of the Fe II/CaT ratio as a function of redshift, suggesting the effect of a recent starburst that enhanced the α-elements with respect to iron at intermediate redshift. Hence, the Fe II/CaT ratio could be used to map the metal and the star formation in AGNs. The Fe II/CaT ratio is also highlighted by the PCA, pointing out the relevance of the metal content in our sample. The negative correlation with the Eddington ratio corroborated by the bootstrap analysis supports the Fe II/CaT as a metal indicator instead of the typical Fe II/Mg II λ2800 ratio used for this purpose. However, a more complete sample and sources at large redshift are needed to verify these results.

We are grateful to the anonymous referee for her/his comments and suggestions that helped to improve the manuscript. The project was partially supported by the National Science Centre, Poland, grant No. 2017/26/A/-ST9/00756 (Maestro 9), and by the Ministry of Science and Higher Education (MNiSW) grant DIR/WK/2018/-12. D.D. acknowledges support from grant PAPIIT UNAM, 113719.

Software: `CLOUDY` v17.01 (Ferland et al. 2017); `MATPLOTLIB` (Hunter 2007); NUMPY (Oliphant 2015); `SKLEARN` (Pedregosa et al. 2011); `STATSMODELS` (Seabold & Perktold 2010); `TOPCAT` (Taylor 2005).

Appendix A
Tables

In this section, we summarize the observational properties of the full sample employed in the analysis. The description of the columns is included in the notes of each table.

Table A1
Observational Parameters

Object	z	log L_{opt} (erg s^{-1})	log L_{NIR} (erg s^{-1})	R_{FeII}	R_{CaT}	FWHM Hβ (km s^{-1})	FWHM OI (km s^{-1})	FWMH CaII (km s^{-1})	EW Hβ (Å)	EW OI (Å)	EW CaII (Å)	EW FeII (Å)
(1)	(2)	(3)	(4)	(5)	(6)	(7)	(8)	(9)	(10)	(11)	(12)	(13)
Persson (1988) Sample												
I Zw 1†	0.061	44.684 ± 0.048	44.694 ± 0.049	1.78 ± 0.05	0.51 ± 0.13	950 ± 100	600 ± 150	1150 ± 150	66 ± 5	13 ± 1	43 ± 4	119 ± 12
Mrk 42	0.025	43.299 ± 0.048	43.247 ± 0.049	1.07 ± 0.07	0.41 ± 0.14	500 ± 100	450 ± 150	800 ± 150	36 ± 2	13 ± 1	19 ± 2	40 ± 6
Mrk 478†	0.077	44.685 ± 0.048	44.607 ± 0.049	0.93 ± 0.06	0.23 ± 0.07	1250 ± 100	1100 ± 150	2500 ± 200	78 ± 5	18 ± 2	28 ± 3	77 ± 10
II Zw 136	0.063	44.47 ± 0.048	44.424 ± 0.049	0.66 ± 0.05	0.17 ± 0.13	1850 ± 100	1200 ± 150	2300 ± 250	96 ± 7	25 ± 3	29 ± 6	68 ± 7
Mrk 231	0.044	44.456 ± 0.048	44.59 ± 0.049	2.46 ± 0.05	0.42 ± 0.19	5700 ± 100	3500 ± 150	1900 ± 250	50 ± 4	36 ± 5	53 ± 5	120 ± 10
3C 273	0.159	46.097 ± 0.048	45.833 ± 0.049	0.40 ± 0.05	0.12 ± 0.04	3800 ± 100	1900 ± 150	2250 ± 250	89 ± 6	22 ± 5	27 ± 5	40 ± 4
Mrk 6	0.019	43.556 ± 0.048	43.675 ± 0.049	0.83 ± 0.16	0.47 ± 0.43	2800 ± 200	1650 ± 200	1950 ± 200	29 ± 6	5 ± 2	15 ± 6	24 ± 7
Mrk 486	0.039	43.969 ± 0.048	43.892 ± 0.049	0.27 ± 0.06	0.07 ± 0.04	1450 ± 100	1450 ± 150	1300 ± 250	105 ± 5	23 ± 3	12 ± 6	31 ± 4
Mrk 1239†	0.02	43.158 ± 0.048	44.2 ± 0.049	1.10 ± 0.07	0.11 ± 0.07	750 ± 100	950 ± 150	1550 ± 400	95 ± 5	25 ± 3	10 ± 5	103 ± 15
Mrk 766	0.013	43.468 ± 0.048	43.221 ± 0.049	0.68 ± 0.12	0.31 ± 0.25	700 ± 100	1050 ± 150	1450 ± 300	44 ± 3	12 ± 2	11 ± 5	29 ± 8
Zw 0033 + 45	0.047	44.352 ± 0.048	44.159 ± 0.049	0.53 ± 0.10	0.16 ± 0.08	2300 ± 200	2050 ± 200	2600 ± 400	110 ± 10	23 ± 4	27 ± 3	60 ± 12
Mrk 684	0.046	44.161 ± 0.048	44.2 ± 0.049	1.29 ± 0.07	0.16 ± 0.10	1300 ± 100	850 ± 150	850 ± 250	38 ± 4	5 ± 2	8 ± 4	51 ± 7
Mrk 335†	0.026	43.974 ± 0.048	43.932 ± 0.049	⩽0.417	⩽0.025	1450 ± 100	1000 ± 150	⋯	86 ± 5	17 ± 2	⩽5	40 ± 6
Mrk 376	0.056	44.367 ± 0.048	44.367 ± 0.049	0.62 ± 0.06	0.05 ± 0.03	5800 ± 100	4500 ± 200	⋯	101 ± 10	28 ± 6	10 ± 5	67 ± 7
Mrk 493†	0.032	43.678 ± 0.048	43.356 ± 0.049	0.78 ± 0.06	0.21 ± 0.18	450 ± 100	450 ± 150	650 ± 300	41 ± 3	7 ± 1	11 ± 8	33 ± 4
Mrk 841	0.037	44.124 ± 0.048	44.045 ± 0.049	⩽0.209	⩽0.032	4950 ± 100	3300 ± 150	⋯	107 ± 6	21 ± 3	7 ± 0	25 ± 6
Ton 1542	0.063	44.207 ± 0.048	44.404 ± 0.049	⩽0.363	⩽0.05	3800 ± 100	2850 ± 250	⋯	114 ± 11	24 ± 3	8 ± 0	43 ± 4
VII Zw 118	0.079	44.697 ± 0.048	44.63 ± 0.049	⩽0.447	⩽0.076	3700 ± 100	2600 ± 300	⋯	90 ± 9	14 ± 2	5 ± 0	38 ± 4
Mrk 124	0.057	43.592 ± 0.048	44.073 ± 0.049	⩽0.708	⩽0.078	1050 ± 100	1050 ± 250	⋯	76 ± 8	20 ± 4	7 ± 0	55 ± 6
Mrk 9	0.04	44.155 ± 0.048	43.915 ± 0.049	⩽0.398	⩽0.036	3450 ± 100	2500 ± 250	⋯	104 ± 10	21 ± 2	7 ± 0	45 ± 5
NGC 7469	0.016	43.864 ± 0.048	43.863 ± 0.049	⩽0.339	⩽0.045	2700 ± 200	1750 ± 250	⋯	72 ± 7	11 ± 2	4 ± 0	25 ± 4
Akn 120	0.034	44.188 ± 0.048	44.62 ± 0.049	⩽0.468	⩽0.062	6300 ± 100	4900 ± 400	⋯	89 ± 5	22 ± 4	7 ± 0	42 ± 4
Mrk 352	0.014	43.037 ± 0.048	43.136 ± 0.049	⩽0.219	⩽0.048	3750 ± 100	3250 ± 300	⋯	83 ± 5	19 ± 4	6 ± 0	19 ± 4
Mrk 304	0.066	44.507 ± 0.048	44.416 ± 0.049	⩽0.282	⩽0.017	3300 ± 200	3300 ± 400	⋯	118 ± 6	11 ± 2	4 ± 0	36 ± 6
Mrk 509	0.034	44.508 ± 0.048	44.43 ± 0.049	⩽0.129	⩽0.041	6000 ± 200	2500 ± 200	⋯	125 ± 6	28 ± 3	10 ± 0	18 ± 3
Martínez-Aldama et al. (2015a, 2015b) Sample												
HE 1349 + 0007	1.444	47.119 ± 0.047	46.887 ± 0.045	0.692 ± 0.143	0.234 ± 0.086	5027 ± 430	4580 ± 680	4530 ± 940	33.5 ± 4	19.9 ± 4	24.7 ± 7	18.5 ± 1
HE 1409 + 0101	1.65	47.629 ± 0.044	47.264 ± 0.048	1.549 ± 0.107	0.316 ± 0.066	4000 ± 160	3100 ± 310	3550 ± 500	26.8 ± 1	15.3 ± 2	19.9 ± 6	36.2 ± 2
HE 2349−3800	1.604	47.11 ± 0.044	46.933 ± 0.045	0.832 ± 0.057	0.288 ± 0.093	4000 ± 160	3480 ± 520	3520 ± 700	27.1 ± 1	17.6 ± 4	19.9 ± 6	19.9 ± 1
HE 2147−3212	1.543	47.163 ± 0.049	46.891 ± 0.045	1.479 ± 0.375	0.49 ± 0.079	4491 ± 660	4300 ± 860	3990 ± 150	28.4 ± 3	22.1 ± 6	47.4 ± 4	35 ± 4
HE 2202−2557	1.535	47.172 ± 0.048	46.585 ± 0.043	0.537 ± 0.062	0.117 ± 0.019	7000 ± 540	5810 ± 1060	5900 ± 330	27.4 ± 1	3.6 ± 1	13 ± 3	12.7 ± 1
HE 2340−4443	0.922	46.758 ± 0.046	46.674 ± 0.049	0.224 ± 0.021	0.089 ± 0.064	3200 ± 100	3430 ± 220	3190 ± 1700	77.5 ± 3	15.9 ± 1	14.8 ± 10	15.4 ± 1
HE 0248−3628	1.536	47.465 ± 0.045	47.222 ± 0.044	0.372 ± 0.034	0.251 ± 0.023	3800 ± 150	3490 ± 260	3990 ± 150	40.7 ± 2	12.2 ± 2	31.3 ± 2	13.6 ± 0.5
HE 2352−4010	1.58	47.727 ± 0.044	47.537 ± 0.05	0.447 ± 0.031	0.17 ± 0.023	2900 ± 90	1930 ± 110	3080 ± 180	45.3 ± 1	16.6 ± 2	21.7 ± 3	17.6 ± 0.3
HE 0035−2853	1.638	47.309 ± 0.048	47.177 ± 0.044	1.479 ± 0.17	0.447 ± 0.041	5141 ± 390	5000 ± 370	4540 ± 170	30.3 ± 1	9.4 ± 2	27.9 ± 2	40.7 ± 3
HE 0048−2804	0.847	46.032 ± 0.049	46.168 ± 0.044	0.617 ± 0.114	0.102 ± 0.075	5484 ± 470	4990 ± 270	5170 ± 2400	40.1 ± 4	18.4 ± 1	4.9 ± 3	22.3 ± 2
HE 0058−3231	1.582	47.336 ± 0.048	47.043 ± 0.055	0.589 ± 0.176	0.389 ± 0.09	5127 ± 160	4960 ± 100	4910 ± 760	55.4 ± 2	44.4 ± 8	59.6 ± 14	27.7 ± 2
HE 0203−4627	1.438	47.102 ± 0.048	46.941 ± 0.045	0.759 ± 0.192	0.479 ± 0.088	5486 ± 810	6000 ± 250	5960 ± 530	26.1 ± 3	13.6 ± 3	33.2 ± 3	14.4 ± 2
HE 0005−2355	1.412	47.161 ± 0.047	46.863 ± 0.045	0.933 ± 0.237	0.166 ± 0.107	4777 ± 710	3500 ± 820	4600 ± 1070	21.8 ± 2	7.8 ± 2	13.9 ± 8	17.2 ± 2
HE 0043−2300	1.54	47.409 ± 0.05	47.257 ± 0.045	0.316 ± 0.044	0.214 ± 0.025	3511 ± 110	4000 ± 360	4000 ± 150	69.3 ± 5	24.5 ± 3	36.1 ± 3	20 ± 1
HE 0349−5249	1.541	47.567 ± 0.047	46.826 ± 0.049	1.704 ± 0.102	0.165 ± 0.014	4000 ± 400	3810 ± 220	4000 ± 150	21.9 ± 2.4	13.5 ± 3	37.6 ± 8	32.1 ± 3.5
HE 0359−3959	1.521	47.132 ± 0.047	46.911 ± 0.049	1.173 ± 0.07	0.371 ± 0.031	4000 ± 400	1770 ± 320	1560 ± 60	40.6 ± 4.4	9.2 ± 2.1	46.6 ± 9.9	43.3 ± 4.7
HE 0436−3709	1.445	46.949 ± 0.062	46.855 ± 0.046	1.164 ± 0.07	0.335 ± 0.028	4491 ± 449	4440 ± 250	4610 ± 170	33.8 ± 3.7	13.9 ± 1.9	26.8 ± 5.7	33.7 ± 3.7

Table A1
(Continued)

Object	z	log L_{opt} (erg s^{-1})	log L_{NIR} (erg s^{-1})	R_{FeII}	R_{CaT}	FWHM Hβ (km s^{-1})	FWHM OI (km s^{-1})	FWMH CaII (km s^{-1})	EW Hβ (Å)	EW OI (Å)	EW CaII (Å)	EW FeII (Å)
(1)	(2)	(3)	(4)	(5)	(6)	(7)	(8)	(9)	(10)	(11)	(12)	(13)
HE 0507−3236	1.577	47.094 ± 0.044	46.939 ± 0.063	0.291 ± 0.006	0.119 ± 0.034	3200 ± 320	2830 ± 420	3870 ± 800	71.3 ± 7.2	25.1 ± 6.1	23.4 ± 8.2	17.8 ± 1.8
HE 0512−3329	1.587	47.222 ± 0.044	47.095 ± 0.064	0.81 ± 0.017	0.24 ± 0.05	3800 ± 380	2170 ± 320	2320 ± 360	75.6 ± 7.6	26.7 ± 6.5	46.6 ± 13.4	53.5 ± 5.4
HE 0926−0201	1.682	47.572 ± 0.049	47.338 ± 0.054	1.139 ± 0.082	0.374 ± 0.033	2900 ± 290	4310 ± 380	4500 ± 170	27.6 ± 3.1	28.9 ± 4.3	33.1 ± 7	27.6 ± 3.1
HE 1039−0724	1.458	47.027 ± 0.049	46.882 ± 0.05	0.289 ± 0.021	0.033 ± 0.018	5141 ± 514	3810 ± 890	3970 ± 920	28.4 ± 3.2	11.5 ± 3.4	2.7 ± 1.6	6.7 ± 0.8
HE 1120 + 0154	1.472	47.568 ± 0.047	47.363 ± 0.052	0.204 ± 0.012	0.084 ± 0.011	5498 ± 550	4030 ± 230	4040 ± 220	31 ± 3.4	13.3 ± 1.9	8.1 ± 1.9	5.4 ± 0.6
Marinello et al. (2016) Sample												
1H 1934−063†	0.011	42.624 ± 0.043	42.637 ± 0.044	1.404 ± 0.223	0.368 ± 0.047	1430 ± 100	1000 ± 80	1205 ± 84	35.3 ± 3.5	18.8 ± 1.3	29.4 ± 1.9	53.2 ± 5.1
1H 2107−097†	0.027	43.217 ± 0.043	43.465 ± 0.044	1.047 ± 0.106	0.139 ± 0.019	2530 ± 320	1720 ± 138	1700 ± 136	38 ± 3.4	14.4 ± 1.5	14.2 ± 1.5	34.9 ± 3.6
I Zw 1†	0.061	44.344 ± 0.043	44.195 ± 0.044	2.286 ± 0.199	0.564 ± 0.058	1450 ± 110	820 ± 57	1100 ± 77	38.1 ± 2.9	33.9 ± 1.8	73.4 ± 4.1	84.9 ± 4.9
Mrk 1044†	0.016	43.076 ± 0.043	43.013 ± 0.046	1.181 ± 0.127	0.111 ± 0.016	1570 ± 145	1010 ± 61	1200 ± 72	57.2 ± 5.1	18.9 ± 1.2	24.6 ± 2.1	65.3 ± 5.7
Mrk 1239†	0.019	43.19 ± 0.043	43.366 ± 0.051	1.34 ± 0.147	0.148 ± 0.016	1720 ± 130	1220 ± 98	1240 ± 74	64.3 ± 5.3	23.3 ± 1.9	20.1 ± 2.2	74.8 ± 6.2
Mrk 335†	0.026	43.82 ± 0.043	43.721 ± 0.053	0.818 ± 0.092	0.054 ± 0.007	1715 ± 130	1140 ± 103	1490 ± 119	123.8 ± 7.6	25.2 ± 1.7	11.3 ± 1.1	100.5 ± 8.8
Mrk 478†	0.078	44.258 ± 0.043	44.45 ± 0.044	1.023 ± 0.089	0.514 ± 0.056	1250 ± 100	1300 ± 91	1560 ± 94	76.9 ± 6.1	20.8 ± 1.7	19.9 ± 1.6	55.2 ± 4.9
Mrk 493†	0.032	43.393 ± 0.043	43.515 ± 0.044	1.721 ± 0.179	0.387 ± 0.046	1450 ± 110	770 ± 31	1065 ± 64	62.5 ± 5.9	13.3 ± 1.1	17.5 ± 1.4	33.3 ± 1.8
PG 1448 + 273†	0.065	44.305 ± 0.043	44.064 ± 0.044	1.189 ± 0.129	0.262 ± 0.034	1730 ± 135	880 ± 35	885 ± 44	31.2 ± 3.8	15.2 ± 1	18.8 ± 1.3	32.2 ± 1.8
Tons 180†	0.062	44.283 ± 0.043	43.911 ± 0.058	0.985 ± 0.11	0.145 ± 0.015	1470 ± 135	930 ± 41	990 ± 59	32.3 ± 1.9	9.6 ± 0.7	19.5 ± 1.6	31.1 ± 2.2
Marinello et al. (2020) Sample												
PHL 1092	0.394	44.883 ± 0.043	44.604 ± 0.047	2.576 ± 0.108	0.839 ± 0.038	1850 ± 100	1250 ± 100	3750 ± 360	34.2 ± 2.2	24.4 ± 1.8	90.2 ± 7.1	88.5 ± 5.3

Note. Column (1): object name. Column (2): redshift. Column (3): optical continuum luminosity at 5100 Å. Column (4): NIR luminosity at 8542 Å. Columns (5) and (6): R_{FeII} and **CaT** values, respectively. Columns (7), (8), and (9): FWHM of Hβ, O I λ8446, and **CaT** in units of km s^{-1}, respectively. Columns (10), (11), (12), and (13): equivalent width of Hβ, O I λ8446, **CaT**, and Fe II in units of Å, respectively.

Table A2
Black Hole Parameters

Object	log $M_{\rm BH}$ ($M_\odot$)	log L_{bol}/L_{Edd}
(1)	(2)	(4)
Persson (1988) Sample		
I Zw 1†	$7.935^{+0.177}_{-0.177}$	$-0.362^{+0.184}_{-0.184}$
Mrk 42	$6.966^{+0.257}_{-0.257}$	$-0.501^{+0.262}_{-0.262}$
Mrk 478†	$8.035^{+0.158}_{-0.158}$	$-0.461^{+0.165}_{-0.165}$
II Zw 136	$8.061^{+0.138}_{-0.138}$	$-0.66^{+0.147}_{-0.147}$
Mrk 231	$8.46^{+0.121}_{-0.121}$	$-1.069^{+0.131}_{-0.131}$
3C 273	$9.188^{+0.142}_{-0.14}$	$-0.485^{+0.15}_{-0.148}$
Mrk 6	$7.724^{+0.141}_{-0.141}$	$-1.053^{+0.149}_{-0.149}$
Mrk 486	$7.707^{+0.148}_{-0.148}$	$-0.705^{+0.156}_{-0.156}$
Mrk 1239†	$7.037^{+0.201}_{-0.201}$	$-0.684^{+0.207}_{-0.206}$
Mrk 766	$7.177^{+0.207}_{-0.207}$	$-0.577^{+0.213}_{-0.213}$
Zw 0033 + 45	$8.077^{+0.151}_{-0.151}$	$-0.769^{+0.159}_{-0.159}$
Mrk 684	$7.77^{+0.154}_{-0.154}$	$-0.615^{+0.161}_{-0.161}$
Mrk 335†	$7.709^{+0.148}_{-0.148}$	$-0.704^{+0.156}_{-0.156}$
Mrk 376	$8.419^{+0.121}_{-0.121}$	$-1.099^{+0.131}_{-0.131}$
Mrk 493†	$7.129^{+0.276}_{-0.276}$	$-0.361^{+0.28}_{-0.28}$
Mrk 841	$8.232^{+0.12}_{-0.12}$	$-1.107^{+0.13}_{-0.13}$
Ton 1542	$8.181^{+0.122}_{-0.122}$	$-0.989^{+0.131}_{-0.131}$
VII Zw 118	$8.432^{+0.124}_{-0.124}$	$-0.849^{+0.134}_{-0.134}$
Mrk 124	$7.389^{+0.168}_{-0.168}$	$-0.69^{+0.175}_{-0.175}$
Mrk 9	$8.118^{+0.123}_{-0.123}$	$-0.968^{+0.132}_{-0.132}$
NGC 7469	$7.875^{+0.142}_{-0.142}$	$-0.957^{+0.15}_{-0.15}$
Akn 120	$8.353^{+0.121}_{-0.121}$	$-1.177^{+0.13}_{-0.13}$
Mrk 352	$7.553^{+0.126}_{-0.126}$	$-1.297^{+0.136}_{-0.135}$
Mrk 304	$8.289^{+0.135}_{-0.135}$	$-0.858^{+0.144}_{-0.144}$
Mrk 509	$8.506^{+0.125}_{-0.125}$	$-1.074^{+0.134}_{-0.134}$
Martínez-Aldama et al. (2015a, 2015b) Sample		
HE 1349 +0007	$9.834^{+0.183}_{-0.179}$	$-0.313^{+0.189}_{-0.185}$
HE 1409 +0101	$10.023^{+0.178}_{-0.173}$	$-0.094^{+0.184}_{-0.179}$
HE 2349−3800	$9.746^{+0.166}_{-0.162}$	$-0.233^{+0.172}_{-0.168}$
HE 2147−3212	$9.817^{+0.219}_{-0.216}$	$-0.260^{+0.225}_{-0.222}$
HE 2202−2557	$9.981^{+0.181}_{-0.177}$	$-0.418^{+0.188}_{-0.184}$
HE 2340−4443	$9.479^{+0.157}_{-0.154}$	$-0.246^{+0.164}_{-0.160}$

Table A2
(Continued)

Object	log $M_{\rm BH}$ ($M_\odot$)	log L_{bol}/L_{Edd}
(1)	(2)	(4)
HE 0248−3628	$9.917^{+0.174}_{-0.169}$	$-0.119^{+0.180}_{-0.175}$
HE 2352−4010	$9.960^{+0.180}_{-0.175}$	$0.048^{+0.185}_{-0.180}$
HE 0035−2853	$9.943^{+0.183}_{-0.178}$	$-0.270^{+0.189}_{-0.185}$
HE 0048−2804	$9.286^{+0.163}_{-0.161}$	$-0.634^{+0.171}_{-0.169}$
HE 0058−3231	$9.956^{+0.169}_{-0.165}$	$-0.262^{+0.176}_{-0.172}$
HE 0203−4627	$9.856^{+0.219}_{-0.216}$	$-0.348^{+0.224}_{-0.222}$
HE 0005−2355	$9.838^{+0.220}_{-0.217}$	$-0.283^{+0.226}_{-0.223}$
HE 0043−2300	$9.859^{+0.172}_{-0.167}$	$-0.106^{+0.179}_{-0.175}$
HE 0349−5249	$9.990^{+0.199}_{-0.195}$	$-0.110^{+0.205}_{-0.201}$
HE 0359−3959	$9.758^{+0.190}_{-0.187}$	$-0.227^{+0.196}_{-0.193}$
HE 0436−3709	$9.703^{+0.188}_{-0.185}$	$-0.317^{+0.198}_{-0.195}$
HE 0507−3236	$9.658^{+0.190}_{-0.186}$	$-0.156^{+0.195}_{-0.192}$
HE 0512−3329	$9.788^{+0.192}_{-0.188}$	$-0.184^{+0.197}_{-0.193}$
HE 0926−0201	$9.877^{+0.201}_{-0.196}$	$0.007^{+0.207}_{-0.203}$
HE 1039−0724	$9.793^{+0.188}_{-0.185}$	$-0.345^{+0.195}_{-0.191}$
HE 1120+0154	$10.105^{+0.200}_{-0.195}$	$-0.225^{+0.205}_{-0.201}$
Marinello et al. (2016) Sample		
1H 1934−063†	$6.985^{+0.156}_{-0.155}$	$-1.059^{+0.162}_{-0.161}$
1H 2107−097†	$7.507^{+0.178}_{-0.178}$	$-1.107^{+0.183}_{-0.183}$
I Zw 1†	$7.907^{+0.151}_{-0.151}$	$-0.605^{+0.158}_{-0.158}$
Mrk 1044†	$7.259^{+0.162}_{-0.162}$	$-0.973^{+0.168}_{-0.167}$
Mrk 1239†	$7.353^{+0.151}_{-0.15}$	$-0.975^{+0.157}_{-0.157}$
Mrk 335†	$7.688^{+0.148}_{-0.148}$	$-0.805^{+0.155}_{-0.155}$
Mrk 478†	$7.807^{+0.156}_{-0.156}$	$-0.575^{+0.162}_{-0.162}$
Mrk 493†	$7.399^{+0.152}_{-0.152}$	$-0.859^{+0.158}_{-0.158}$
PG 1448 + 273†	$7.949^{+0.15}_{-0.149}$	$-0.679^{+0.156}_{-0.156}$
Tons 180†	$7.879^{+0.16}_{-0.16}$	$-0.626^{+0.166}_{-0.166}$
Marinello et al. (2020) Sample		
PHL 1092	$8.281^{+0.140}_{-0.140}$	$-0.549^{+0.147}_{-0.147}$

Note. Column (1): object name. Column (2): black hole mass estimated using the classical RL relation (Equation (3)), in units of $M_\odot$. Column (3): Eddington ratio.

Table A3
Parameters of the Correlations for the Observed and Bootstrap Sample

Relation		Observational Data					Bootstrap Results						
(1)		α (2)	β (3)	ρ (4)	p-value (5)	σ (6)	α_{BS} (7)	β_{BS} (8)	ρ_{BS} (9)	f_{sig} (10)	P. Dist. (11)	p-value$_{ran}$ (12)	f_{ran} (13)
$EW_{H\beta}$	L_{opt}	-0.064 ± 0.032	4.632 ± 1.469	-0.412	0.001	0.200	-0.064 ± 0.031	4.618 ± 1.408	$-0.428^{+0.21}_{-0.17}$	0.5	c,a,b	0.76,0.95, 0.67	3.5×10^{-3}
	L_{NIR}	-0.064 ± 0.036	4.627 ± 1.618	-0.352	0.007	0.204	-0.065 ± 0.034	4.656 ± 1.430	$-0.372^{+0.22}_{-0.17}$	0.2	c,c,d	0.76,0.98,0.60	1.0×10^{-3}
	M_{BH}	-0.091 ± 0.053	2.508 ± 0.455	-0.390	0.002	0.206	-0.092 ± 0.048	2.519 ± 0.409	$-0.405^{+0.24}_{-0.19}$	0.4	c,b,d	0.76,0.96,0.94	1.0×10^{-3}
	L_{bol}/L_{Edd}	$\mathbf{-0.332 \pm 0.149}$	$\mathbf{1.53 \pm 0.102}$	-0.531	1.78×10^{-5}	0.195	$\mathbf{-0.335 \pm 0.148}$	$\mathbf{1.529 \pm 0.09}$	$\mathbf{-0.544}$ $\{C\}^{+0.19}_{-0.16}\{C\}$	0.85	c,c	0.76,0.61	1.5×10^{-3}
EW_{OI}	L_{opt}	-0.007 ± 0.034	1.557 ± 1.548	-0.015	0.910	0.211	-0.007 ± 0.033	1.000 ± 1.510	$-0.016^{+0.23}_{-0.27}$	0.0	e,a,b	0.97,0.95,0.67	1.0×10^{-3}
	L_{NIR}	-0.003 ± 0.037	1.358 ± 1.673	0.053	0.691	0.211	-0.003 ± 0.034	1.358 ± 1.603	$0.060^{+0.20}_{-0.28}$	0.0	e,c,d	0.97,0.98,0.60	1.5×10^{-3}
	M_{BH}	-0.006 ± 0.054	1.271 ± 0.468	-0.008	0.951	0.211	-0.005 ± 0.057	1.264 ± 0.459	$0.008^{+0.23}_{-0.27}$	0.0	e,b,d	0.97,0.96,0.94	1.0×10^{-3}
	L_{bol}/L_{Edd}	-0.079 ± 0.161	1.172 ± 0.110	-0.162	0.223	0.209	-0.082 ± 0.142	1.169 ± 0.107	$-0.161^{+0.23}_{-0.26}$	0.0	e,c	0.97,0.61	5.0×10^{-4}
EW_{FeII}	L_{opt}	-0.091 ± 0.039	5.666 ± 1.754	-0.409	0.001	0.239	-0.092 ± 0.039	5.678 ± 1.705	$-0.422^{+0.22}_{-0.17}$	0.5	a,a,b	0.94,0.95,0.67	5.0×10^{-4}
	L_{NIR}	-0.095 ± 0.042	5.846 ± 1.917	-0.367	0.005	0.242	-0.096 ± 0.043	5.881 ± 1.809	$-0.385^{+0.23}_{-0.18}$	0.3	a,c,d	0.94,0.95,0.55	5.0×10^{-4}
	M_{BH}	$\mathbf{-0.151 \pm 0.06}$	$\mathbf{2.831 \pm 0.52}$	-0.493	8.58×10^{-5}	0.234	$\mathbf{-0.15 \pm 0.059}$	$\mathbf{2.824 \pm 0.52}$	$\mathbf{-0.517}$ $\{C\}^{+0.21}_{-0.14}\{C\}$	0.75	a,b,d	0.94,0.96,0.94	1.0×10^{-3}
	L_{bol}/L_{Edd}	-0.281 ± 0.203	1.373 ± 0.139	-0.360	0.005	0.265	-0.279 ± 0.211	1.374 ± 0.142	$-0.375^{+0.22}_{-0.19}$	0.3	a,c	0.94,0.61	5.0×10^{-4}
EW_{CaT}	L_{opt}	0.068 ± 0.053	-1.851 ± 2.381	0.417	0.001	0.324	0.069 ± 0.049	-1.896 ± 1.842	$0.425^{+0.14}_{-0.25}$	0.5	a,a,b	0.93,0.95,0.67	1.0×10^{-3}
	L_{NIR}	0.068 ± 0.057	-1.827 ± 2.593	0.377	0.004	0.327	0.069 ± 0.051	-1.878 ± 2.451	$0.380^{+0.15}_{-0.24}$	0.3	a,c,d	0.93,0.98, 0.60	1.5×10^{-3}
	M_{BH}	0.088 ± 0.085	0.470 ± 0.733	0.301	0.022	0.331	0.089 ± 0.074	0.456 ± 0.608	$0.305^{+0.17}_{-0.23}$	0.1	a,b,d	0.93,0.96,0.94	1.0×10^{-3}
	L_{bol}/L_{Edd}	$\mathbf{0.428 \pm 0.237}$	$\mathbf{1.477 \pm 0.162}$	0.482	$\mathbf{1.27 \times 10^{-4}}$	0.309	$\mathbf{0.431 \pm 0.200}$	$\mathbf{1.477 \pm 0.133}$	$\mathbf{0.494}^{+0.14}_{-0.24}$	0.71	a,c	0.93,0.61	$\mathbf{1.0 \times 10^{-3}}$
R_{FeII}	L_{opt}	-0.015 ± 0.049	0.520 ± 2.209	-0.063	0.640	0.301	-0.015 ± 0.045	0.536 ± 1.901	$-0.064^{+0.22}_{-0.28}$	0.0	e,a,b	0.96,0.95,0.67	1.5×10^{-3}
	L_{NIR}	-0.017 ± 0.053	0.631 ± 2.383	-0.081	0.546	0.301	-0.017 ± 0.047	0.602 ± 2.264	$-0.083^{+0.22}_{-0.26}$	0.0	e,c,d	0.96,0.98,0.60	5.0×10^{-4}
	M_{BH}	-0.042 ± 0.076	0.204 ± 0.662	-0.162	0.226	0.299	-0.042 ± 0.065	0.205 ± 0.566	$-0.160^{+0.22}_{-0.25}$	0.0	e,b,d	0.96,0.96,0.94	2.0×10^{-3}
	L_{bol}/L_{Edd}	0.109 ± 0.230	-0.092 ± 0.157	0.105	0.432	0.300	0.111 ± 0.239	-0.088 ± 0.141	$0.102^{+0.25}_{-0.29}$	0.0	e,c	0.96,0.61	1.0×10^{-3}
R_{CaT}	L_{opt}	0.057 ± 0.063	-3.392 ± 2.846	0.247	0.061	0.388	0.056 ± 0.056	-3.350 ± 2.437	$0.243^{+0.18}_{-0.23}$	0.1	f,a,b	0.76,0.95,0.67	3.5×10^{-3}
	L_{NIR}	0.059 ± 0.068	-3.476 ± 3.079	0.240	0.069	0.389	0.060 ± 0.058	-3.502 ± 2.823	$0.241^{+0.18}_{-0.24}$	0.1	f,c,d	0.76,0.98,0.60	1.5×10^{-3}
	M_{BH}	0.058 ± 0.101	-1.309 ± 0.874	0.117	0.381	0.394	0.058 ± 0.091	-1.306 ± 0.762	$0.111^{+0.20}_{-0.24}$	0.0	f,b,d	0.76,0.96,0.94	1.5×10^{-3}
	L_{bol}/L_{Edd}	$\mathbf{0.500 \pm 0.275}$	$\mathbf{-0.516 \pm 0.188}$	0.425	$\mathbf{8.90 \times 10^{-4}}$	0.359	$\mathbf{0.498 \pm 0.254}$	$\mathbf{-0.516 \pm 0.152}$	$0.426^{+0.18}_{-0.25}$	0.51	f,c	0.76,0.61	$\mathbf{5.0 \times 10^{-4}}$
Fe II/CaT	L_{opt}	$\mathbf{-0.072 \pm 0.039}$	$\mathbf{3.912 \pm 1.78}$	-0.441	$\mathbf{5.31 \times 10^{-4}}$	0.242	$\mathbf{-0.071 \pm 0.039}$	$\mathbf{3.877 \pm 1.747}$	$\mathbf{-0.444}$ $\{C\}^{+0.22}_{-0.22}\{C\}$	0.54	e,a,b	0.98,0.95,0.67	$\mathbf{5.0 \times 10^{-4}}$
	L_{NIR}	$\mathbf{-0.077 \pm 0.043}$	$\mathbf{4.107 \pm 1.929}$	-0.456	3.20×10^{-4}	0.244	$\mathbf{-0.076 \pm 0.042}$	$\mathbf{4.086 \pm 1.887}$	$\mathbf{-0.470}$ $\{C\}^{+0.23}_{-0.20}\{C\}$	0.61	e,c,d	0.98,0.98,0.60	$\mathbf{5.0 \times 10^{-4}}$
	M_{BH}	-0.100 ± 0.064	1.513 ± 0.552	-0.354	0.006	0.249	-0.102 ± 0.061	1.532 ± 0.559	$-0.348^{+0.23}_{-0.24}$	0.3	e,b,d	0.98,0.96,0.94	1.5×10^{-3}
	L_{bol}/L_{Edd}	$\mathbf{-0.391 \pm 0.179}$	$\mathbf{0.424 \pm 0.122}$	-0.554	$\mathbf{6.44 \times 10^{-6}}$	0.233	$\mathbf{-0.394 \pm 0.164}$	$\mathbf{0.422 \pm 0.099}$	$\mathbf{-0.560}$ $\{C\}^{+0.20}_{-0.17}\{C\}$	0.89	e,c	0.98,0.61	$\mathbf{1.0 \times 10^{-3}}$
R_{FeII}	R_{CaT}	$\mathbf{0.973 \pm 0.239}$	$\mathbf{-0.657 \pm 0.081}$	0.721	1.75×10^{-10}	0.270	$\mathbf{0.974 \pm 0.189}$	$\mathbf{-0.658 \pm 0.07}$	$0.737^{+0.07}_{-0.19}$	1.0	e,f	0.96,0.76	2.0×10^{-3}

Note. Column (1): relations. Column (2): slope of the observational sample and error at 2σ. Column (3): ordinate of the observational sample and error at 2σ. Column (4): Spearman rank correlation coefficient for the observational sample. Significant correlations with respect to this parameter are in boldface. Column (5): p-value of the correlation coefficient. Column (6): Scatter of the observational sample with respect to the best fit. Column (7): slope of the bootstrap sample and error at 2σ. Column (8): ordinate of the bootstrap sample and error at 2σ. Column (9): maximum of Spearman rank correlation coefficient distribution for 1000 realizations of the bootstrap sample and the errors at 2σ. Column (10): fraction of significant bootstrap realizations with respect to the total number. Column (11): probability distributions used to model the observational distributions using a random sample. The symbols are as follows: a–skewnorm, b–powernorm, c–powerlaw, d–loglaplace, e–powerlognorm, f–lognorm. The symbols follow the order of Column (1). In correlations involving luminosity and black hole mass, two distributions were used in the modeling. Column (12): p-value of the Kolmogorov−Smirnov test to select the best distribution fitting. Order is the same as in Column (11). Column (13): fraction of significant correlations assuming two random samples.

Table A4
Correlations between the First Four Eigenvectors and the Physical Parameters

Relations		Full		Low L		High L	
		ρ	p-value	ρ	p-value	ρ	p-value
(1)		(2)	(3)	(4)	(5)	(6)	(7)
PC1	$FWHM_{H\beta}$	**−0.792**	$\mathbf{1.32 \times 10^{-13}}$	**0.669**	$\mathbf{7.37 \times 10^{-5}}$	**0.76**	$\mathbf{1.73 \times 10^{6}}$
	$FWHM_{OI}$	**−0.845**	$\mathbf{7.51 \times 10^{-17}}$	**0.728**	$\mathbf{7.65 \times 10^{-6}}$	**0.884**	$\mathbf{2.1 \times 10^{-10}}$
	$FWHM_{CaT}$	**−0.844**	$\mathbf{1.77 \times 10^{-13}}$	0.659	0.00159	**0.85**	$\mathbf{3.94 \times 10^{-8}}$
	$EW_{H\beta}$	**0.583**	$\mathbf{1.59 \times 10^{-6}}$	**0.736**	$\mathbf{5.46 \times 10^{-6}}$	**−0.694**	$\mathbf{2.93 \times 10^{-5}}$
	EW_{OI}	0.180	0.177	**0.871**	$\mathbf{8.11 \times 10^{-10}}$	−0.296	0.12
	EW_{FeII}	**0.703**	$\mathbf{7.79 \times 10^{-10}}$	0.476	0.00897	**−0.681**	$\mathbf{4.73 \times 10^{-5}}$
	EW_{CaT}	−0.179	0.178	−0.072	0.712	−0.257	0.178
	z	**−0.700**	$\mathbf{1 \times 10^{-9}}$	0.356	0.0578	0.366	0.0512
	$\log L_{bol}$	**−0.748**	$\mathbf{1.49 \times 10^{-11}}$	0.495	0.00638	0.458	0.0124
	$\log M_{BH}$	**−0.845**	$\mathbf{6.99 \times 10^{-17}}$	**0.701**	$\mathbf{2.24 \times 10^{-5}}$	**0.662**	$\mathbf{9.16 \times 10^{-5}}$
	$\log L_{bol}/L_{Edd}$	**−0.519**	$\mathbf{2.94 \times 10^{-5}}$	−0.492	0.00672	0.174	0.367
	$\log R_{FeII}$	0.164	0.218	−0.316	0.0952	−0.089	0.645
	$\log R_{CaT}$	−0.151	0.259	−0.382	0.041	−0.021	0.914
	log Fe II/CaT	**0.426**	$\mathbf{8.46 \times 10^{-4}}$	0.338	0.073	−0.125	0.518
PC2	$FWHM_{H\beta}$	0.023	0.864	−0.344	0.0674	−0.278	0.145
	$FWHM_{OI}$	−0.033	0.804	−0.38	0.0422	0.057	0.769
	$FWHM_{CaT}$	−0.098	0.518	0.456	0.0435	−0.016	0.939
	$EW_{H\beta}$	−0.012	0.93	−0.212	0.27	−0.327	0.0835
	EW_{OI}	**−0.681**	$\mathbf{3.92 \times 10^{-9}}$	0.348	0.064	0.346	0.0661
	EW_{FeII}	**−0.509**	$\mathbf{4.57 \times 10^{-5}}$	**0.66**	$\mathbf{9.88 \times 10^{-5}}$	0.357	0.0572
	EW_{CaT}	**−0.81**	$\mathbf{1.29 \times 10^{-14}}$	**0.855**	$\mathbf{3.57 \times 10^{-9}}$	**0.86**	$\mathbf{2.3 \times 10^{-9}}$
	z	−0.291	0.0267	0.069	0.722	0.5	0.00569
	$\log L_{bol}$	−0.268	0.0416	0.065	0.738	0.492	0.00666
	$\log M_{BH}$	−0.169	0.205	−0.233	0.223	0.306	0.106
	$\log L_{bol}/L_{Edd}$	0.272	0.0392	0.354	0.0598	0.492	0.00669
	$\log R_{FeII}$	**−0.46**	$\mathbf{2.79 \times 10^{-4}}$	**0.698**	$\mathbf{2.6 \times 10^{-5}}$	**0.669**	$\mathbf{7.26 \times 10^{-5}}$
	$\log R_{CaT}$	**−0.506**	$\mathbf{5.08 \times 10^{-5}}$	**0.65**	$\mathbf{1.34 \times 10^{-4}}$	**0.838**	$\mathbf{1.46 \times 10^{-8}}$
	log Fe II/CaT	0.225	0.0888	−0.257	0.178	−0.338	0.0725
PC3	$FWHM_{H\beta}$	**−0.512**	$\mathbf{3.97 \times 10^{-5}}$	0.196	0.308	−0.046	0.812
	$FWHM_{OI}$	**−0.506**	$\mathbf{5.15 \times 10^{-5}}$	−0.036	0.852	0.074	0.701
	$FWHM_{CaT}$	**−0.47**	$\mathbf{9.7 \times 10^{-4}}$	−0.244	0.301	0.042	0.837
	$EW_{H\beta}$	**−0.647**	$\mathbf{4.18 \times 10^{-8}}$	**−0.743**	$\mathbf{3.87 \times 10^{-6}}$	0.478	0.00874
	EW_{OI}	**−0.562**	$\mathbf{4.39 \times 10^{-6}}$	−0.342	0.0693	**0.83**	$\mathbf{2.57 \times 10^{-8}}$
	EW_{FeII}	0.027	0.838	−0.244	0.202	−0.104	0.59
	EW_{CaT}	0.318	0.0149	0.251	0.189	0.065	0.739
	z	−0.007	0.959	0.023	0.905	0.119	0.54
	$\log L_{bol}$	−0.041	0.761	0.14	0.469	0.02	0.916
	$\log M_{BH}$	−0.195	0.142	0.185	0.337	−0.064	0.741
	$\log L_{bol}/L_{Edd}$	0.341	0.00884	−0.124	0.521	0.097	0.617
	$\log R_{FeII}$	**0.621**	$\mathbf{2 \times 10^{-7}}$	0.4	0.0313	−0.501	0.00564
	$\log R_{CaT}$	**0.600**	$\mathbf{6.52 \times 10^{-7}}$	0.486	0.00759	−0.173	0.368
	log Fe II/CaT	−0.232	0.0794	−0.351	0.0621	−0.478	0.00875
PC4	$FWHM_{H\beta}$	0.279	0.034	−0.096	0.619	0.378	0.0431
	$FWHM_{OI}$	0.190	0.154	−0.187	0.332	0.313	0.0985
	$FWHM_{CaT}$	0.118	0.435	**−0.699**	$\mathbf{6.02 \times 10^{-4}}$	0.423	0.0313
	$EW_{H\beta}$	−0.381	0.00315	−0.054	0.78	−0.1	0.608
	EW_{OI}	−0.339	0.00934	0.075	0.698	0.017	0.929
	EW_{FeII}	0.130	0.331	0.041	0.832	0.164	0.397
	EW_{CaT}	0.076	0.571	−0.19	0.324	0.153	0.43
	z	−0.089	0.506	−0.189	0.327	−0.423	0.0224
	$\log L_{bol}$	−0.057	0.67	−0.266	0.163	−0.469	0.0104
	$\log M_{BH}$	0.016	0.907	−0.197	0.307	−0.281	0.14
	$\log L_{bol}/L_{Edd}$	−0.239	0.0708	−0.07	0.717	**−0.693**	$\mathbf{3.13 \times 10^{-5}}$
	$\log R_{FeII}$	0.42	0.00104	0.018	0.927	0.268	0.16
	$\log R_{CaT}$	0.207	0.119	−0.279	0.143	0.18	0.35
	log Fe II/CaT	0.224	0.0915	0.361	0.0547	0.244	0.201

Note. Column (1): relations. Columns (2), (4), and (6): Spearman rank correlation coefficient for the full, low-L, and high-L samples, respectively. Columns (3), (5), and (7): p-value of the correlation coefficient, for the full, low-L, and high-L samples, respectively. Significant correlations are in boldface.

Appendix B
Random Distribution and Residuals Plots

In this section are included extra figures that are complementary to the results in Sections 4.5 and 4.6. Figure B1 shows the distributions of Fe II/CaT and L_{bol}/L_{Edd} parameters compared with the ones from a fitting process; see Section 4.5.1. The fitted distribution and p-value are indicated in the left and middle panels. The right panel shows the distribution of a random sample to get a significant correlation Fe II/CaT$-L_{bol}/L_{Edd}$ as high as the one from the observational sample.

In order to assess any signatures of redshift effects, Figures B2 and B3 show the distributions of the residuals as a function of the redshift for low- and high-L objects. This division is in agreement with low- and high-redshift sources. The median of each distribution (dashed vertical lines) does not show a significant difference from the zero residual levels. Hence, there is not a dependence within the 2σ confidence level. This suggests that the relations in Figures 3 and 4 are not artificially enhanced by redshift effects.

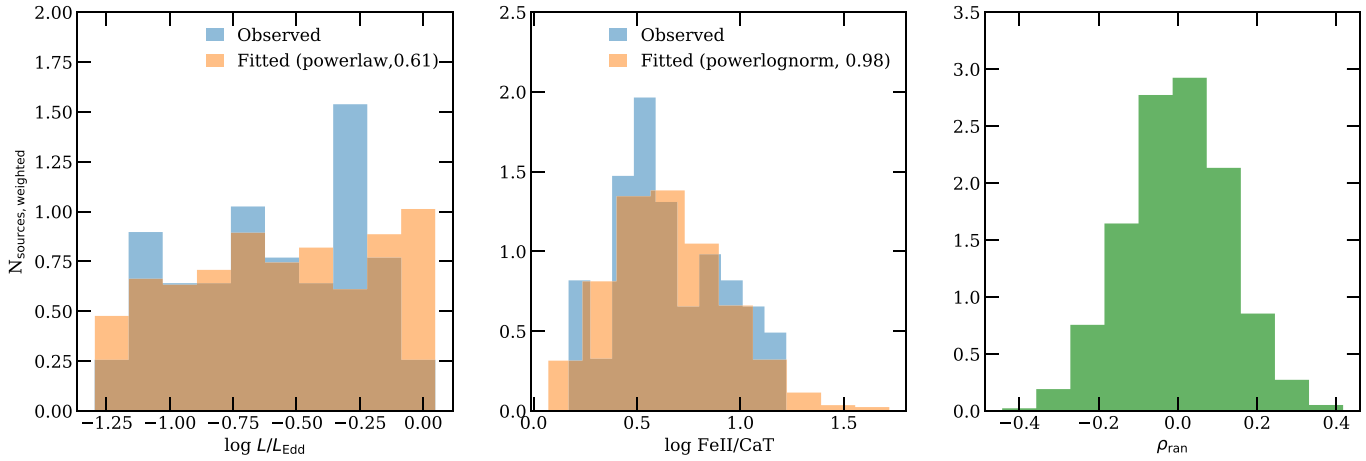

Figure B1. Modeled probability distribution for L_{bol}/L_{Edd} (left panel) and Fe II/CaT (middle panel) parameters. The blue distribution corresponds to the observed one, while the red one is obtained via a bootstrap analysis; see Section 4.5.1. The right panel shows the distribution of the Spearman rank correlation coefficient for 58 randomly selected sources from the distribution in the left and middle panels. The number of significant correlations ($\rho_{\rm ran}$ and $p-{\rm val}<0.001$) is below the 3σ confidence level.

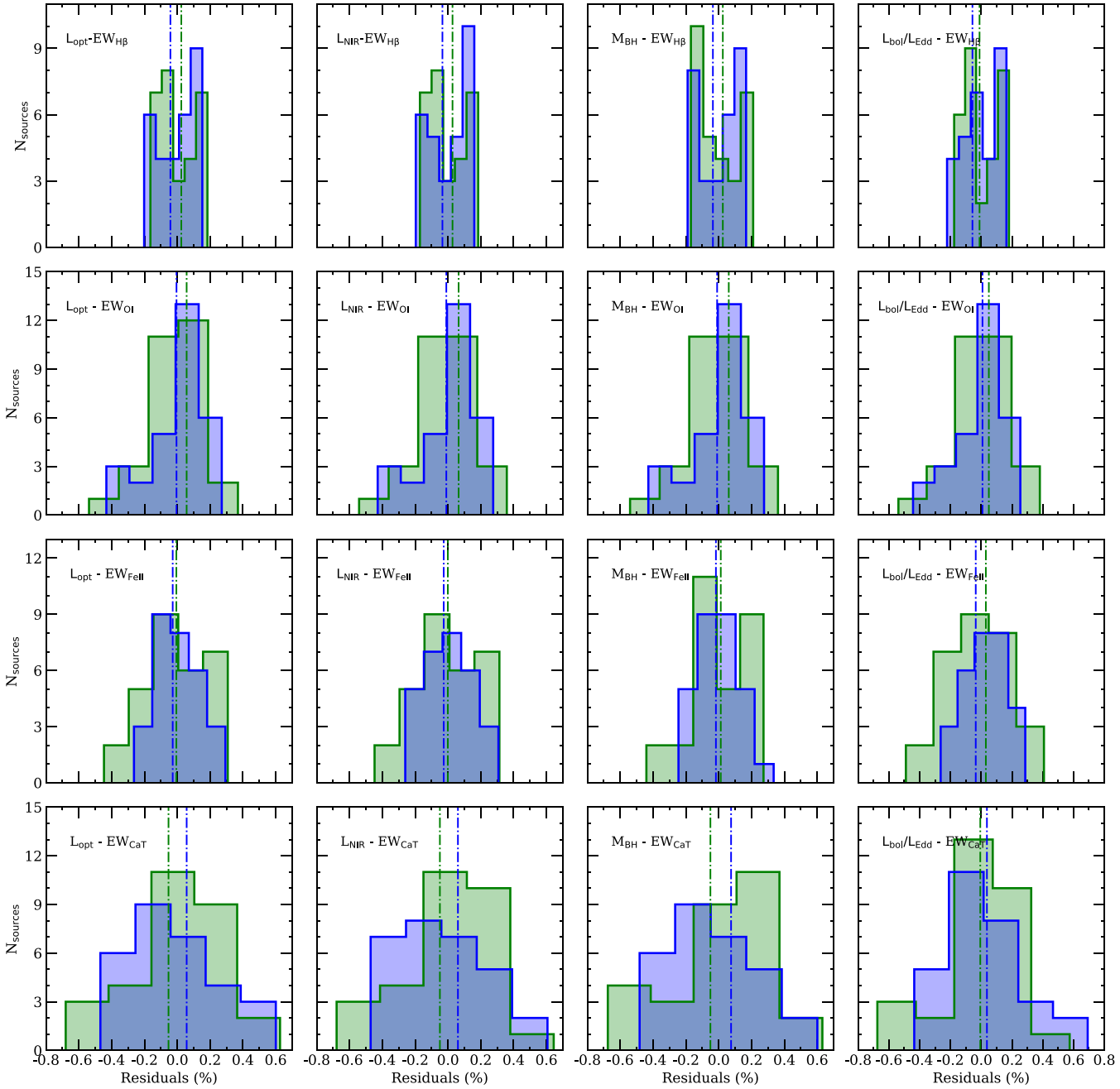

Figure B2. Distribution of the residuals with respect to the best fits as a function of redshift for the correlation shown in Figure 3. In each panel is indicated the analyzed relation. The green distribution corresponds to the low-L (and low-z) subsample, while the blue one draws the high-L (and high-z) distributions. Vertical lines indicate the median of each distribution.

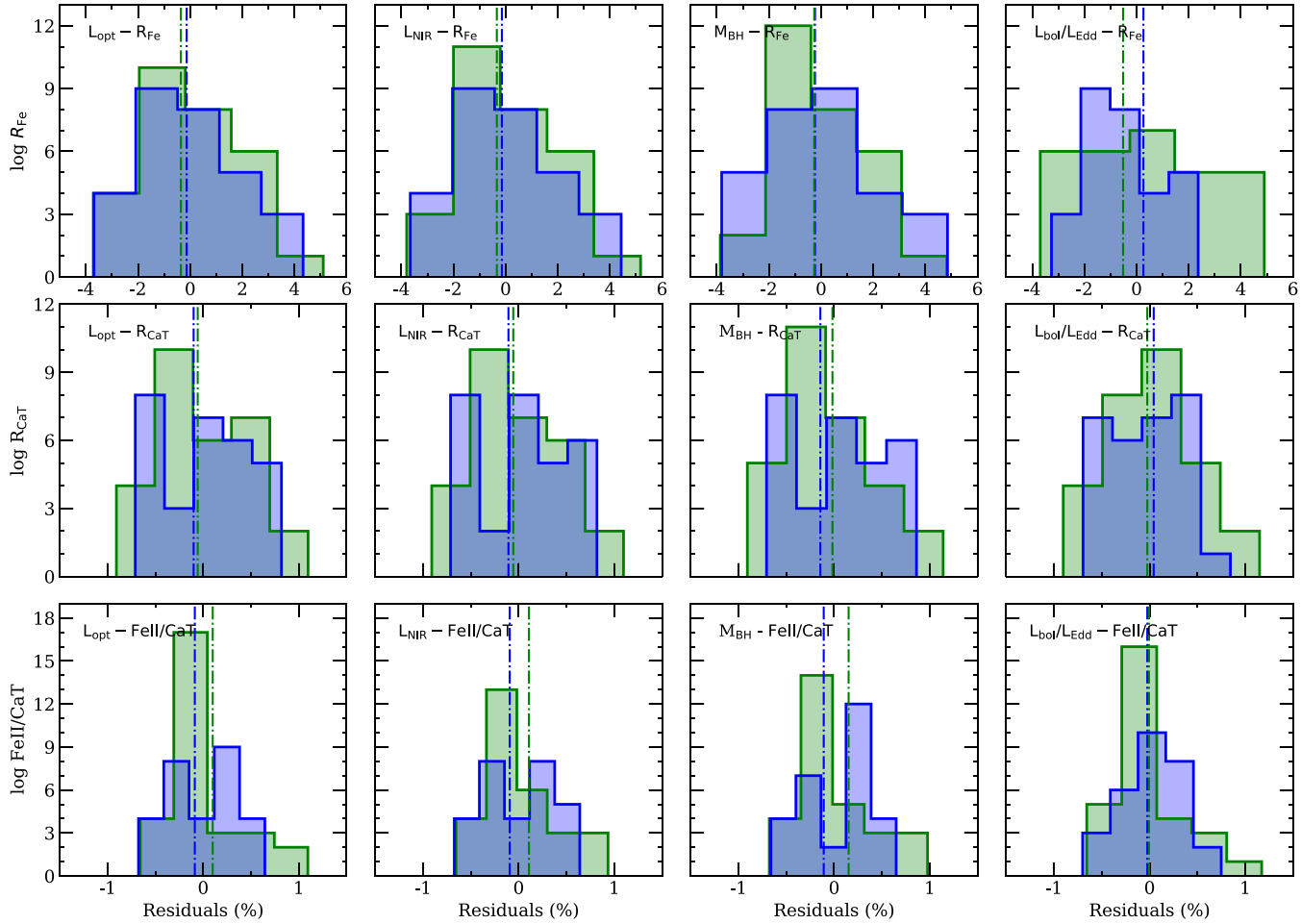

Figure B3. Same as Figure B2, but for correlations shown in Figure 4.

Appendix C
Principal Component Analysis—Effect of Redundant Parameters

The correlation between a variable and a principal component (PC) is used as the coordinates of the variable on the PC. The representation of variables differs from the plot of the observations: the observations are represented by their projections, but the variables are represented by their correlations (Abdi & Williams 2010): (a) positively correlated variables are grouped together; (b) negatively correlated variables are positioned on opposite sides of the plot origin (opposed quadrants); and (c) the distance between variables and the origin measures the quality of the variables on the factor map. Variables that are away from the origin are well represented on the factor map.

As a first test for the PCA, we consider the aforementioned 11 parameters. Before drawing any definitive conclusions, we wanted to remove parameters that are redundant/uncorrelated. This allows us to eliminate noise in the PCA output due to the presence of these redundant/uncorrelated variables. We perform this testing in two steps. In the first step, we analyze the effect of the presence of both optical and NIR luminosity in the PCA run. The optical (at 5100 Å) and the NIR (8542 Å) luminosities are almost identical for our sample (see bottom right panel of Figure 2) with a correlation coefficient $r = 0.950$ (p-value $= 6.72 \times 10^{-30}$). This result is synchronous to our PCA (Figure C1). Here, the factor maps for the two cases (with and without optical luminosity) are shown adjacent to each other. At a first glance, the differences in the sources constituting our full sample can be clearly seen. The (3) Persson and (4) Marinello samples (i.e., the low-luminosity sources) are similarly oriented in the PC1–PC2 diagram (factor map), while the high-luminosity sources from the two catalogs from Martinez-Aldama (1 and 2) occupy a separate region in the factor map. We study these subsamples in more detail in the next section. The corresponding scree plots are similar and highlight the dominance of the first PC (43% for the case with optical luminosity, and 40.6% for the case without it). The subsequent PCs show similar precedence. We thus make use of only the NIR luminosity henceforth.

The parameters $R_{\rm FeII}$ and $R_{\rm CaT}$ are estimated from the various observations that are tabulated in Table A1. These values are estimated from the ratio of the fluxes of the respective emission species (optical Fe II within the 4434–4684 Å and Hβ; CaT and Hβ, respectively). In our analysis, we use the EWs for the said species, which are basically scaled versions of the line fluxes, one that is normalized by the corresponding continuum luminosity (at 5100 Å for Fe II and 8542 Å for CaT). Thus, the $R_{\rm FeII}$ and $R_{\rm CaT}$ seemingly become redundant in the presence of the EWs. We test this effect of redundancy on our sample, and

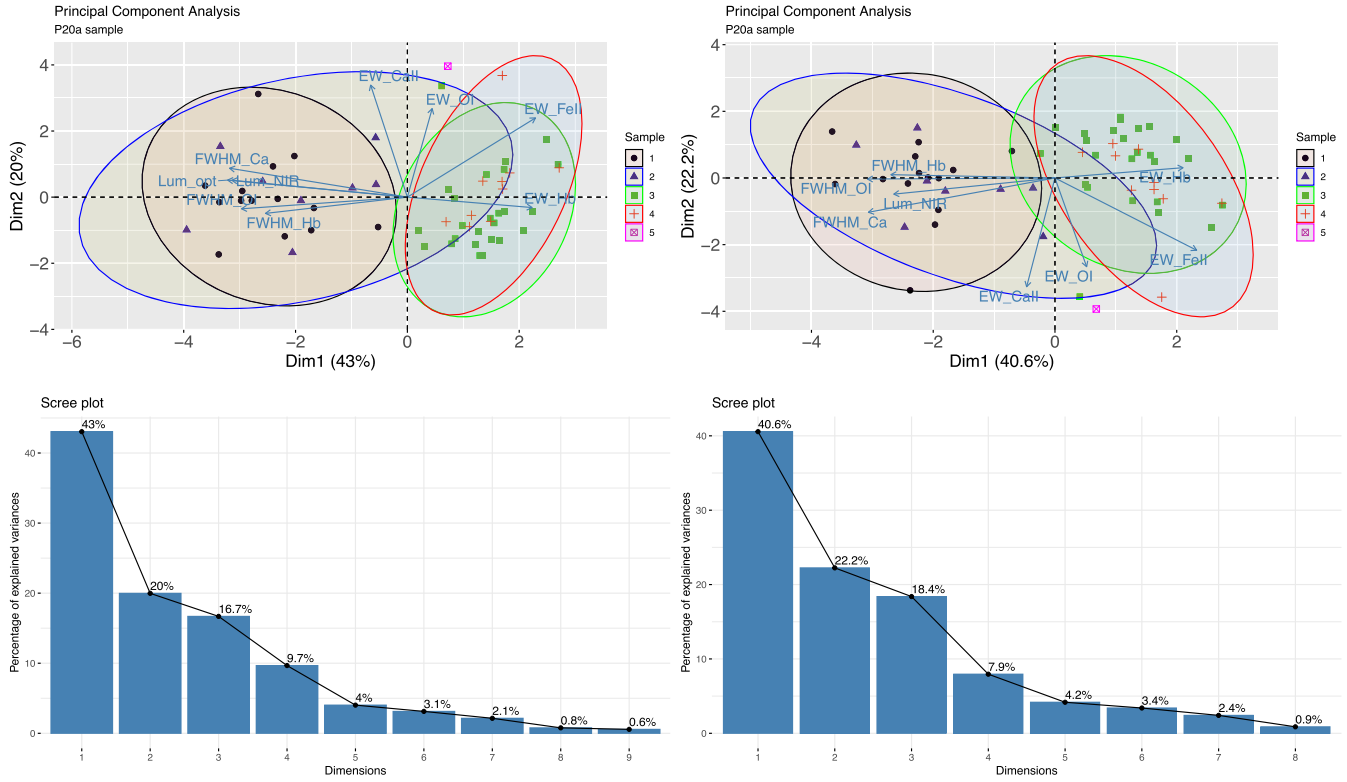

Figure C1. Graphical representation of the PCA decomposition of our sample (58 sources). The circles represent individual objects on the standardized PC1–PC2 plane that have variables indicated by the axis labels. The arrows represent the prominence of the variables in the PC1–PC2 plane. The dashed lines mark the coordinate axes in the PC1–PC2 plane, and the ellipses depict the 95% occupancy of the sources in their respective subsamples. The sample is categorized based on their original source catalogs (see Panda et al. 2020a, for details on the observational sample)—(1) Martínez-Aldama et al. (2015a); (2) Martínez-Aldama et al. (2015b); (3) Persson (1988); (4) Marinello et al. (2016); and (5) PHL1092 (Marinello et al. 2020). Left: with $L_{\rm opt}$; Right: without $L_{\rm opt}$. The bottom panels illustrate the precedence of the first 10 PCs in the form of scree plots.

the results are presented in Figure C2. The representation is similar to that in Figure C1. The factor map on the left panel shows the case where the $R_{\rm FeII}$ and $R_{\rm CaT}$ are included in the analysis. Here, the $R_{\rm CaT}$ vector is completely aligned with the EW(CaT) vector, suggesting that the quantity is strongly dependent on this variable itself and is less affected by the EW(Hβ). On the other hand, the orientation of the $R_{\rm FeII}$ vector suggests that the quantity is affected by both EW(Fe II) and EW(Hβ). The corresponding scree plots for the two cases highlight the importance of the noise introduced in the PCA due to the presence of $R_{\rm FeII}$ and $R_{\rm CaT}$. In the case where these variables were used, the data set is organized such that the two PCs are almost identical (32.8% for PC1 and 31.7% for PC2). This gives a false impression that the data set is driven by a 2D plane rather than a line. A similar aspect of the optical main sequence being represented as a line or a plane was explored in Wildy et al. (2019). On the other hand, when these two variables are removed and the PCA module is rerun, we see that the data set is dominated by the variance along the first PC (40.6%) and the second PC becomes less important (22.2%). Another effect of the removal of redundant variables is the emergence of other quantities, e.g., EW(O I λ8446).

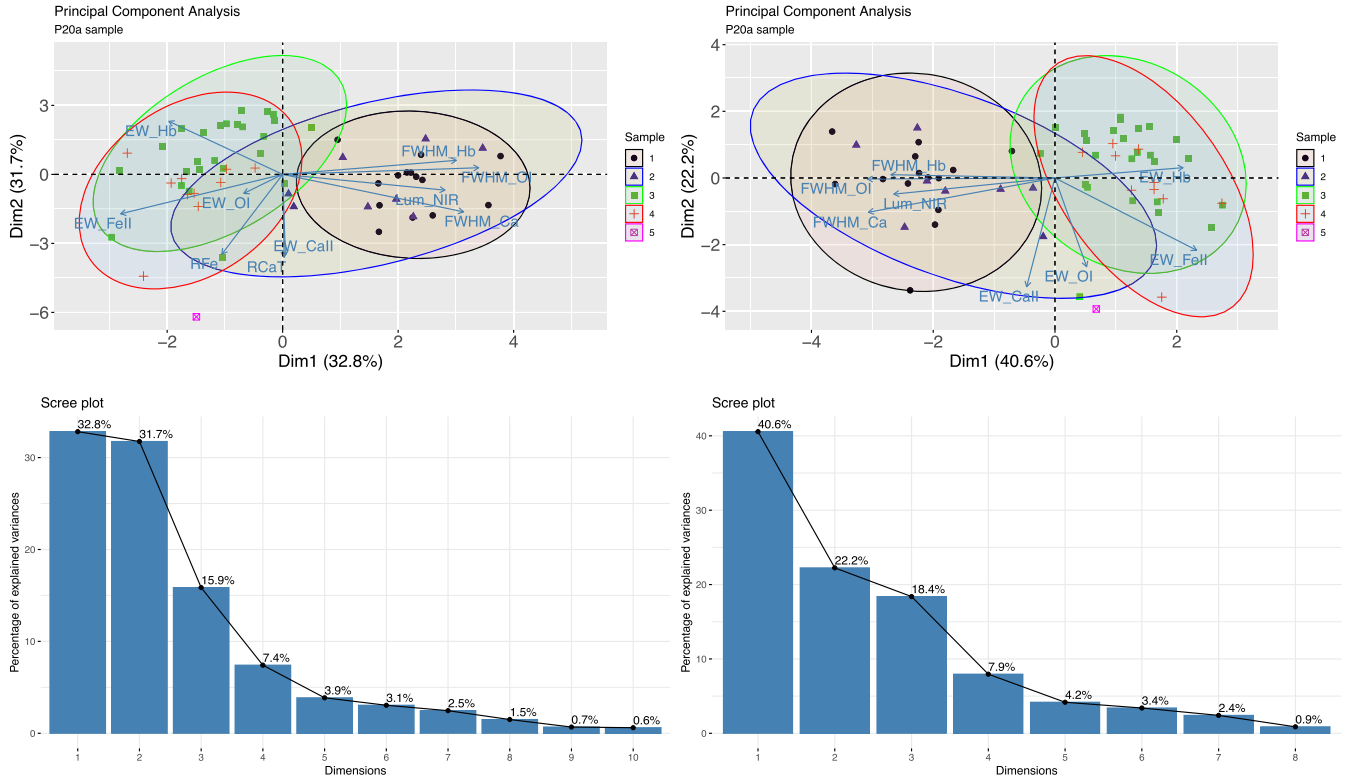

Figure C2. Similar to Figure C1. Left: with $R_{\rm FeII}$ and $R_{\rm CaT}$; right: without $R_{\rm FeII}$ and $R_{\rm CaT}$. The bottom panels illustrate the precedence of the first 10 PCs in the form of scree plots.

These two tests further confirm that the results of the PCA are dependent on the selection of the sample and the chosen properties (Kuraszkiewicz et al. 2009).

Appendix D
Principal Component Analysis—Low- and High-luminosity Samples

Taking note from the previous runs and the heterogeneity present in our sample, we now separate the full sample into two subsamples based on the median of the optical luminosity (at 5100 Å) of the distribution, i.e., log $L_{\rm opt} = 44.49\,{\rm erg\,s^{-1}}$ (Section 4.3.3), which gives 29 sources in each case. We then perform the PCA on each of the subsamples (low $L_{\rm opt}$ and high $L_{\rm opt}$) and illustrate the results in the left and right columns of Figure D1, respectively.

D.1. Low-luminosity Subsample

For the low-luminosity sample, the sources belong to the Persson (19/25) and Marinello (10/10) samples, and the Marinello sample is almost enclosed within the Persson sample in the factor map. The corresponding scree plot shows the dominance of the primary and secondary PCs (41.1% and 30.1%), suggesting that the sample seems to be driven majorly by the combination of the two components that can explain 71.2% of the variance in the data set. Accounting for the subsequent two PCs, 90.6% of the total variation in the data set can be explained in this case.

First PC: Going back to the factor map, we find that the vectors corresponding to the FWHMs of Hβ and O I λ8446 and $\rm EW_{H\beta}$ are co-aligned, with the FWHM vectors having almost similar magnitudes. These two FWHM vectors are also the major contributors to the variance along the primary PC (see third panel in the middle column of Figure 5). For the primary PC, the EW of O I λ8446 follows after these two FWHMs, which then is followed by the NIR luminosity.

Second PC: The factor map highlights the prevalence of the $\rm EW_{CaT}$, followed by the $\rm FWHM_{CaT}$ and the $\rm EW_{FeII}$. This trend is also seen in the contributions to the second PC and supports our original conclusion that the two species Fe II and CaT are similar in terms of their excitation and line emissivities (see fourth panel in the middle column of Figure 5). We expect that the $\rm FWHM_{FeII}$ would show similar behavior, likewise of $\rm FWHM_{CaT}$ (as shown in Marinello et al. 2016, where the authors show an almost perfect correlation between the Fe II emission at 1 μm and CaT) strengthening the inferences from the photoionization modeling (Panda et al. 2020a; Panda 2021). This needs to be tested with a larger, higher signal-to-noise ratio, and more complete sample in the future.

Third and fourth PCs: The third and fourth PCs further contribute to 19.4% of the total variance in the data set. The third PC is singularly dominated by the $\rm EW_{H\beta}$ with a minor contribution from $\rm EW_{CaT}$ and $\rm FWHM_{H\beta}$. Similarly, the fourth PC is mainly driven by the $\rm FWHM_{CaT}$, with only a minor contribution from EW of O I λ8446.

D.2. High-luminosity Subsample

For the high-luminosity sample, the sources belong to the Persson (6/25) and Marinello (PHL1092) samples and all of Martinez-Aldama's sources. The six sources from Persson (Mrk 304, Mrk 509, I Zw 1, Mrk 478, VII Zw 118, and 3C 273) and PHL1092 outline the 95% confidence limit of Martinez-Aldama's sample, shown with the ellipses on the

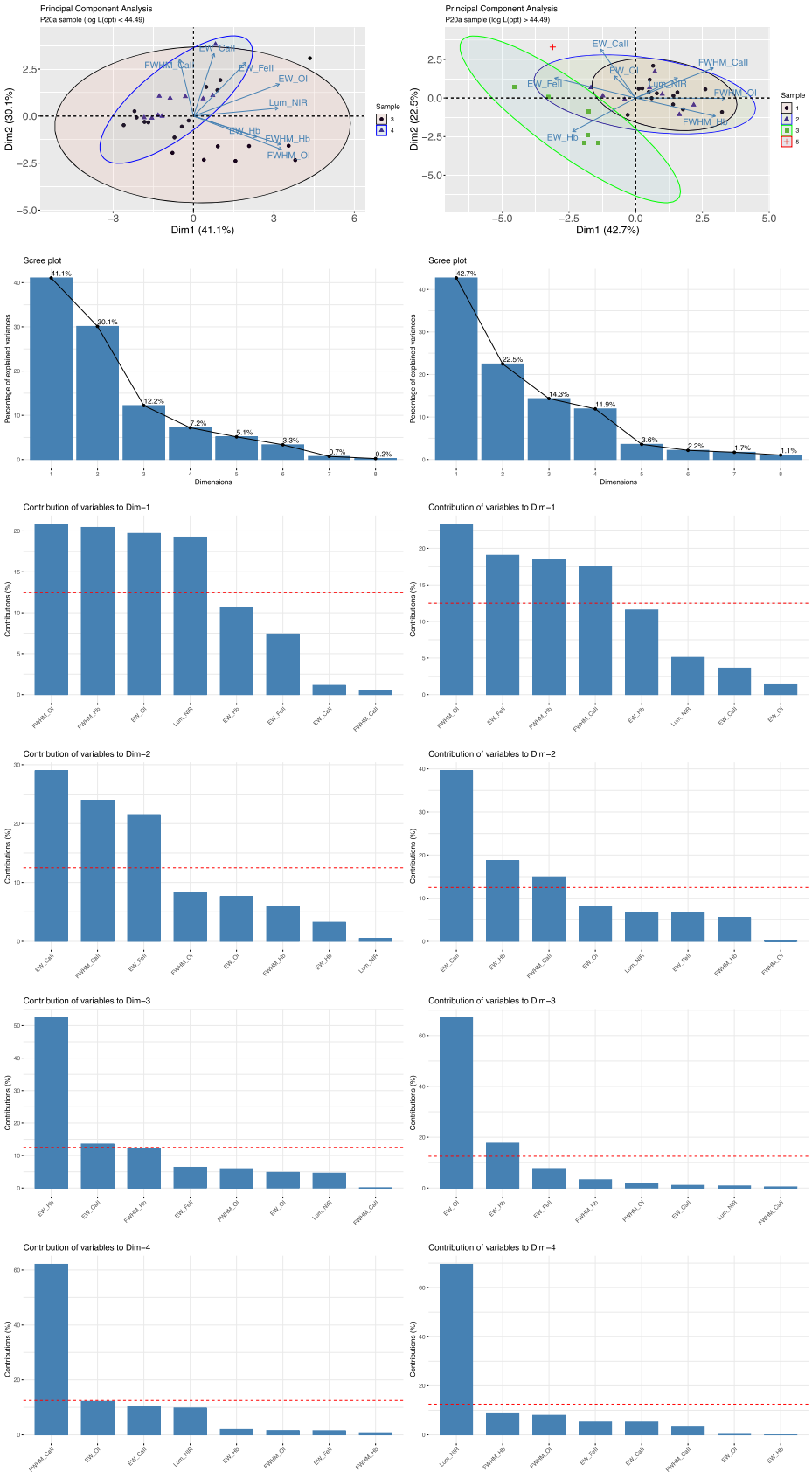

Figure D1. Same as Figure 5. Left: low-luminosity sample (log $L_{\rm opt} \leqslant 44.49$ erg s^{-1}). Right: high-luminosity sample (log $L_{\rm opt} > 44.49$ erg s^{-1}).

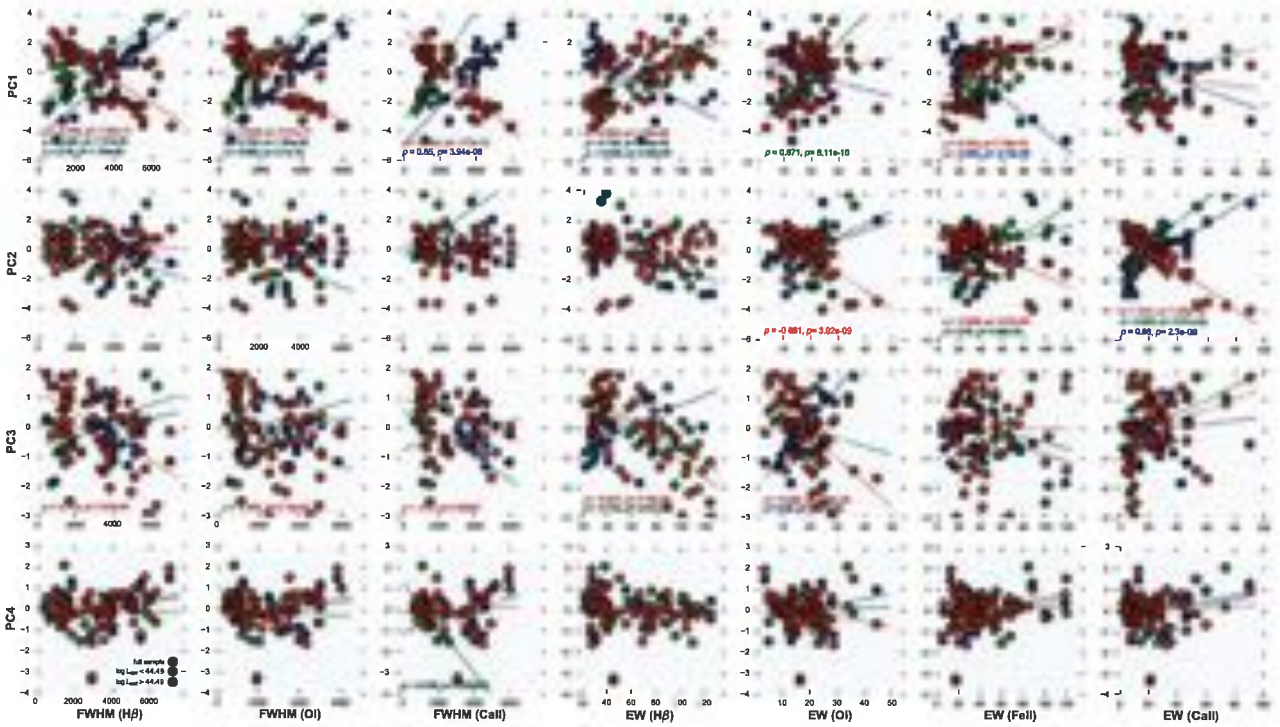

Figure D2. Correlation matrix showing dependence of the first four PCA vectors' loadings vs. the physical parameters (*observed*) for our sample. The sample is divided into low-luminosity (green circles) and high-luminosity (blue circles) subsamples based on the median value of the sample's optical luminosity distribution, i.e., at 44.49 erg s^{-1} (see Appendix D). The full sample is shown with red circles. The Spearman's rank correlation coefficient (ρ) and the p-value are reported for the correlations whenever p-value < 0.001. The OLS fits for each sample are shown using dashed lines with their respective color.

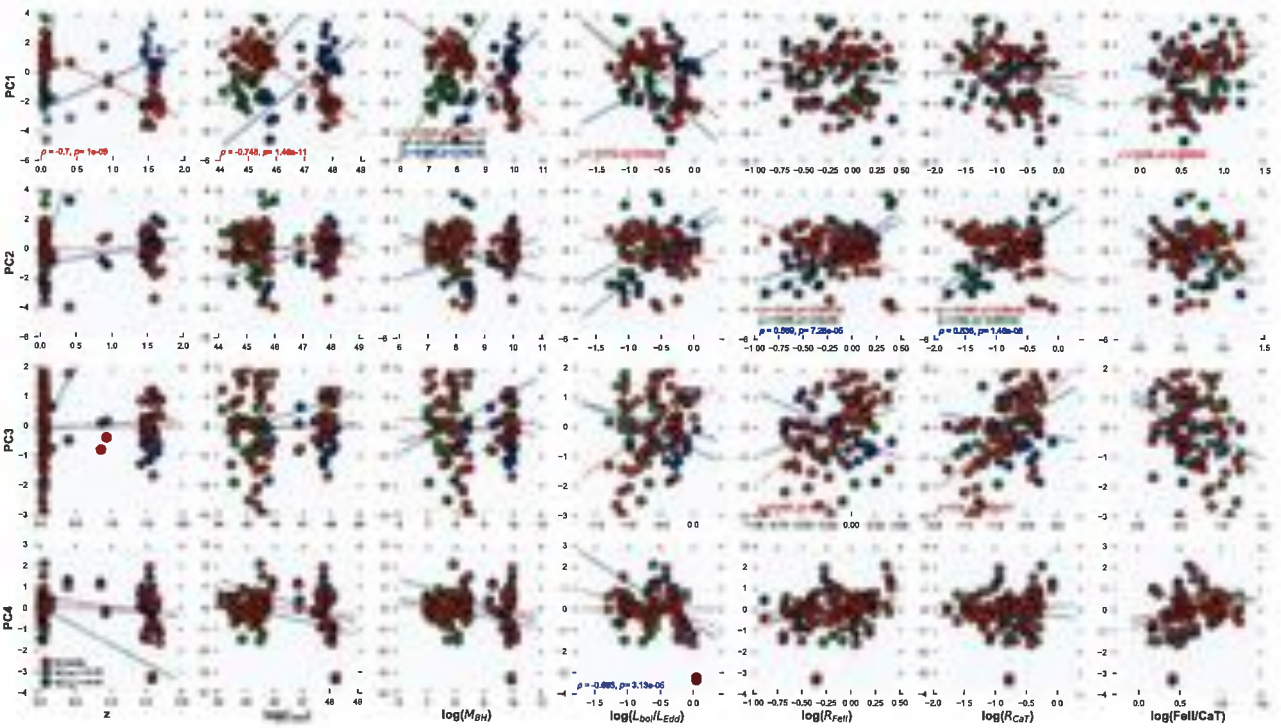

Figure D3. Correlation matrix showing dependence of the first four PCA vectors' loadings vs. the physical parameters (*derived*) for our sample. The colors for the data points are identical to those shown previously in Figure D2. The Spearman's rank correlation coefficients (ρ) and the p-values are reported for the correlations whenever p-value < 0.001. The OLS fits for each sample are shown using dashed lines with their respective color.

factor map (top right panel of Figure 5). This points toward the homogeneity in the subsample as opposed to the earlier scenario when all the sources were bunched together. The corresponding scree plot shows the dominance of the primary and secondary PCs (42.7% and 22.5%), suggesting that the high-luminosity sample behaves similarly to the low-luminosity case. Likewise to the low-luminosity case, accounting for the subsequent two PCs (PC3 and PC4), 91.4% of the total variation in the high-luminosity data set can be explained.

First PC: Compared to the low-luminosity case, the FWHM of O I λ8446 is still the primary dominant driver of the primary PC, followed by the EW_{FeII} $FWHM_{H\beta}$ and $FWHM_{CaT}$. The EW_{FeII} dominates in the negative space of the PC1.

Second PC: The primary contributor to this PC is still EW_{CaT}, but in contrast to the corresponding PC for the low-luminosity case, the EW_{FeII} is rather below the significance threshold in this case. Other significant contributors are the $EW_{H\beta}$, followed by the $FWHM_{CaT}$.

Third and fourth PCs: The third and fourth PCs further contribute to 26.2% (earlier this was 19.4% for the low-luminosity case) of the total variance in the data set. The third PC is dominated by the EW_{OI} with a contribution from $EW_{H\beta}$, whereas the fourth PC is singularly driven by the NIR luminosity.

D.3. Correlations between the Principal Eigenvectors and Observed/Derived Parameters for the Subsamples

In Figure D2, for the PC1, there are significant positive correlations for both the subsamples, especially with respect to $FWHM_{H\beta}$ (low luminosity: $\rho = 0.669$, $p = 7.37 \times 10^{-5}$; high luminosity: $\rho = 0.76$, $p = 1.73 \times 10^{-6}$) and $FWHM_{OI}$ (low luminosity: $\rho = 0.728$, $p = 7.65 \times 10^{-6}$; high luminosity: $\rho = 0.884$, $p = 2.1 \times 10^{-10}$). This is highlighted by the strong correlation between the PC1 and the black hole mass, which is obtained and explained in Figure D3, as the $FWHM_{H\beta}$ is incorporated to estimate the black hole mass. A strong positive correlation is obtained for $FWHM_{CaT}$ ($\rho = 0.85$, $p = 3.94 \times 10^{-8}$) for the high-luminosity subsample. The $EW_{H\beta}$ correlation with PC1 behaves differently for the low-luminosity ($\rho = 0.736$, $p = 5.46 \times 10^{-6}$) and the high-luminosity ($\rho = -0.694$, $p = 2.93 \times 10^{-5}$) samples. The low-luminosity sample follows the trend of the full sample in this case. For EW_{OI}, significant correlation is noted only for the low-luminosity case ($\rho = 0.871$, $p = 8.11 \times 10^{-10}$). For EW_{FeII}, significant anticorrelation is noted only for the high-luminosity case ($\rho = -0.681$, $p = 4.73 \times 10^{-5}$) . For PC2, we have two significant correlations for the low-luminosity case—for EW_{CaT} ($\rho = 0.855$, $p = 3.57 \times 10^{-9}$) and EW_{FeII} ($\rho = 0.66$, $p = 9.88 \times 10^{-5}$). Additionally, there is a correlation obtained for the EW_{CaT} ($\rho = 0.86$, $p = 2.3 \times 10^{-9}$) for the high-luminosity case. For PC3, a significant anticorrelation is observed for the low-luminosity case's $EW_{H\beta}$ ($\rho = -0.743$, $p = 3.87 \times 10^{-6}$) and a significant correlation for the high-luminosity case's EW_{OI} ($\rho = 0.83$, $p = 2.57 \times 10^{-8}$). There is a single significant (anti)correlation observed for PC4, i.e., versus $FWHM_{CaT}$ ($\rho = -0.699$, $p = 6.02 \times 10^{-4}$).

In Figure D3, the strongest and only correlation in the subsamples for the PC1 are with respect to the black hole mass —for the low-luminosity sample, the correlation is relatively stronger ($\rho = 0.701$, $p = 2.24 \times 10^{-5}$) compared to the high-luminosity sample ($\rho = 0.662$, $p = 9.16 \times 10^{-5}$). For PC2, significant correlations are obtained only for R_{FeII} and R_{CaT} cases. For the low-luminosity sample, the correlations of PC2 versus R_{FeII} ($\rho = 0.698$, $p = 2.6 \times 10^{-5}$) and versus R_{CaT} ($\rho = 0.65$, $p = 1.34 \times 10^{-4}$) show a moderate correlation, while for the high-luminosity sample, the correlations of PC2 versus R_{FeII} ($\rho = 0.669$, $p = 7.26 \times 10^{-5}$) and versus R_{CaT} ($\rho = 0.838$, $p = 1.46 \times 10^{-8}$) are slightly stronger. This further corroborates the strong connection between these two parameters from our past results obtained in Paper I and those obtained from the PCA analysis of the full sample in this paper. There are no significant correlations with respect to PC3. The only significant (anti)correlation with respect to PC4 is obtained for L_{Edd} in the high-luminosity sample ($\rho = -0.693$, $p = 3.13 \times 10^{-5}$).

ORCID iDs

Mary Loli Martínez-Aldama https://orcid.org/0000-0002-7843-7689
Swayamtrupta Panda https://orcid.org/0000-0002-5854-7426
Bożena Czerny https://orcid.org/0000-0001-5848-4333
Murilo Marinello https://orcid.org/0000-0001-9719-4523
Paola Marziani https://orcid.org/0000-0002-6058-4912
Deborah Dultzin https://orcid.org/0000-0001-5756-8842

References

Abdi, H., & Williams, L. J. 2010, Wiley Interdiscip. Rev. Comput. Stat., 2, 433
Bachev, R., Marziani, P., Sulentic, J. W., et al. 2004, ApJ, 617, 171
Baldwin, J. A. 1977, ApJ, 214, 679
Baldwin, J. A., Burke, W. L., Gaskell, C. M., & Wampler, E. J. 1978, Natur, 273, 431
Baldwin, J. A., Ferland, G. J., Korista, K. T., Hamann, F., & LaCluyzé, A. 2004, ApJ, 615, 610
Baskin, A., & Laor, A. 2004, MNRAS, 350, L31
Bentz, M. C., Denney, K. D., Grier, C. J., et al. 2013, ApJ, 767, 149
Bessell, M. S. 1990, PASP, 102, 1181
Bizyaev, D., Chen, Y.-M., Shi, Y., et al. 2019, ApJ, 882, 145
Boroson, T. A., & Green, R. F. 1992, ApJS, 80, 109
Collin, S., & Joly, M. 2000, NewAR, 44, 531
Collin, S., Kawaguchi, T., Peterson, B. M., & Vestergaard, M. 2006, A&A, 456, 75
Collin-Souffrin, S., Dyson, J. E., McDowell, J. C., & Perry, J. J. 1988, MNRAS, 232, 539
de Bruyn, A. G., & Sargent, W. L. W. 1978, AJ, 83, 1257
De Rosa, G., Venemans, B. P., Decarli, R., et al. 2014, ApJ, 790, 145
Devereux, N. 2018, MNRAS, 473, 2930
Dietrich, M., Hamann, F., Appenzeller, I., & Vestergaard, M. 2003, ApJ, 596, 817
Dietrich, M., Hamann, F., Shields, J. C., et al. 2002, ApJ, 581, 912
Dong, X.-B., Wang, J.-G., Ho, L. C., et al. 2011, ApJ, 736, 86
Dong, X.-B., Wang, T.-G., Wang, J.-G., et al. 2009, ApJL, 703, L1
Du, P., & Wang, J.-M. 2019, ApJ, 886, 42
Dultzin-Hacyan, D., Taniguchi, Y., & Uranga, L. 1999, in ASP Conf. Ser., 175, Structure and Kinematics of Quasar Broad Line Regions, ed. C. M. Gaskell et al. (San Francisco, CA: ASP), 303
Efron, B., & Tibshirani, R. J. 1993, An Introduction to the Bootstrap, Monographs on Statistics and Applied Probability No. 57 (Boca Raton, FL: Chapman & Hall/CRC)
Ferland, G. J., Chatzikos, M., Guzmán, F., et al. 2017, RMxAA, 53, 385
Ferland, G. J., & Persson, S. E. 1989, ApJ, 347, 656
Garcia-Rissmann, A., Rodríguez-Ardila, A., Sigut, T. A. A., & Pradhan, A. K. 2012, ApJ, 751, 7
Garcia-Rissmann, A., Vega, L. R., Asari, N. V., et al. 2005, MNRAS, 359, 765
Green, P. J., Forster, K., & Kuraszkiewicz, J. 2001, ApJ, 556, 727
Hamann, F., & Ferland, G. 1992, ApJL, 391, L53
Hamann, F., & Ferland, G. 1993, ApJ, 418, 11
Hamann, F., & Ferland, G. 1999, ARA&A, 37, 487
Horne, K., De Rosa, G., Peterson, B. M., et al. 2021, ApJ, 907, 76
Hunter, J. D. 2007, CSE, 9, 90

Jolliffe, I. 2011, in Principal Component Analysis, ed. M. Lovric (Berlin: Springer), 1094
Joly, M. 1987, A&A, 184, 33
Joly, M. 1989, A&A, 208, 47
Kaiser, H. F. 1961, Br. J. Stat. Psychol., 14, 1
Korista, K., Baldwin, J., & Ferland, G. 1998, ApJ, 507, 24
Korista, K., Baldwin, J., Ferland, G., & Verner, D. 1997, ApJS, 108, 401
Koski, A. T. 1978, ApJ, 223, 56
Krawczyk, C. M., Richards, G. T., Mehta, S. S., et al. 2013, ApJS, 206, 4
Kunth, D., & Sargent, W. L. W. 1979, A&A, 76, 50
Kuraszkiewicz, J., Wilkes, B. J., Schmidt, G., et al. 2009, ApJ, 692, 1180
Lusso, E., & Risaliti, G. 2016, ApJ, 819, 154
Madau, P., & Dickinson, M. 2014, ARA&A, 52, 415
Marconi, A., Risaliti, G., Gilli, R., et al. 2004, MNRAS, 351, 169
Marinello, M., Rodríguez-Ardila, A., Garcia-Rissmann, A., Sigut, T. A. A., & Pradhan, A. K. 2016, ApJ, 820, 116
Marinello, M., Rodríguez-Ardila, A., Marziani, P., Sigut, A., & Pradhan, A. 2020, MNRAS, 494, 4187
Martínez-Aldama, M. L., Del Olmo, A., Marziani, P., et al. 2018, FrASS, 4, 65
Martínez-Aldama, M. L., Dultzin, D., Marziani, P., et al. 2015a, ApJS, 217, 3
Martínez-Aldama, M. L., Marziani, P., Dultzin, D., et al. 2015b, JApA, 36, 457
Martínez-Aldama, M. L., Zajaček, M., Czerny, B., & Panda, S. 2020, ApJ, 903, 86
Marziani, P., Bon, E., Bon, N., et al. 2019, Atoms, 7, 18
Marziani, P., Dultzin, D., Sulentic, J. W., et al. 2018, FrASS, 5, 6
Marziani, P., Martínez-Aldama, M. L., Dultzin, D., & Sulentic, J. W. 2014, AstRv, 9, 29
Marziani, P., Sulentic, J. W., Plauchu-Frayn, I., & del Olmo, A. 2013, A&A, 555, A89
Marziani, P., Zamanov, R. K., Sulentic, J. W., & Calvani, M. 2003, MNRAS, 345, 1133
Matteucci, F. 1994, A&A, 288, 57
Matteucci, F., & Recchi, S. 2001, ApJ, 558, 351
Mejía-Restrepo, J. E., Lira, P., Netzer, H., Trakhtenbrot, B., & Capellupo, D. M. 2018, NatAs, 2, 63
Negrete, C. A., Dultzin, D., Marziani, P., et al. 2018, A&A, 620, A118
Negrete, C. A., Dultzin, D., Marziani, P., & Sulentic, J. W. 2014, AdSpR, 54, 1355
Nemmen, R. S., & Brotherton, M. S. 2010, MNRAS, 408, 1598
Netzer, H. 2019, MNRAS, 488, 5185
Oke, J. B., & Shields, G. A. 1976, ApJ, 207, 713
Oliphant, T. 2015, NumPy: A guide to NumPy (2nd edn.; USA: CreateSpace Independent Publishing Platform), http://www.numpy.org/
Onoue, M., Bañados, E., Mazzucchelli, C., et al. 2020, ApJ, 898, 105
Osmer, P. S., Porter, A. C., & Green, R. F. 1994, ApJ, 436, 678
Osmer, P. S., & Shields, J. C. 1999, in ASP Conf. Ser., 162, Quasars and Cosmology, ed. G. Ferland & J. Baldwin (San Francisco, CA: ASP), 235, arXiv:astro-ph/9811459
Osterbrock, D. E. 1976, ApJ, 203, 329
Osterbrock, D. E., & Ferland, G. J. 2006, Astrophysics of Gaseous Nebulae and Active Galactic Nuclei (Sausalito, CA: Iniv. Science Books)
Osterbrock, D. E., & Phillips, M. M. 1977, PASP, 89, 251
Panda, S. 2021, A&A, 650, A154
Panda, S., Czerny, B., Adhikari, T. P., et al. 2018, ApJ, 866, 115
Panda, S., Martínez-Aldama, M. L., Marinello, M., et al. 2020a, ApJ, 902, 76
Panda, S., Marziani, P., & Czerny, B. 2019, ApJ, 882, 79
Panda, S., Marziani, P., & Czerny, B. 2020b, CoSka, 50, 293
Pedregosa, F., Varoquaux, G., Gramfort, A., et al. 2011, JMLR, 12, 2825
Peres-Neto, P. R., Jackson, D. A., & Somers, K. M. 2005, CSDA, 49, 974
Persson, S. E. 1988, ApJ, 330, 751
Pogge, R. W., & Peterson, B. M. 1992, AJ, 103, 1084
Punsly, B., Marziani, P., Berton, M., & Kharb, P. 2020, ApJ, 903, 44
Rakić, N., La Mura, G., Ilić, D., et al. 2017, A&A, 603, A49
Richards, G. T., Lacy, M., Storrie-Lombardi, L. J., et al. 2006, ApJS, 166, 470
Rodriguez-Ardila, A., Garcia Rissmann, A., Sigut, A. A., & Pradhan, A. K. 2012, in Proc. Nuclei of Seyfert galaxies and QSOs—Central engine & conditions of star formation (Bonn: Max-Planck-Insitut für Radioastronomie), 12
Rodríguez-Ardila, A., Viegas, S. M., Pastoriza, M. G., & Prato, L. 2002, ApJ, 565, 140
Runnoe, J. C., Brotherton, M. S., & Shang, Z. 2012a, MNRAS, 422, 478
Runnoe, J. C., Brotherton, M. S., & Shang, Z. 2012b, MNRAS, 426, 2677
Sameshima, H., Yoshii, Y., & Kawara, K. 2017, ApJ, 834, 203
Sameshima, H., Yoshii, Y., Matsunaga, N., et al. 2020, ApJ, 904, 162
Sarkar, A., Ferland, G. J., Chatzikos, M., et al. 2021, ApJ, 907, 12
Schnorr-Müller, A., Davies, R. I., Korista, K. T., et al. 2016, MNRAS, 462, 3570
Seabold, S., & Perktold, J. 2010, in Proc. 9th Python in Science Conf., ed. S. van der Walt & J. Millman (Austin: TX: SciPy), 92
Shemmer, O., & Netzer, H. 2002, ApJL, 567, L19
Shemmer, O., Netzer, H., Maiolino, R., et al. 2004, ApJ, 614, 547
Shen, Y., & Ho, L. C. 2014, Natur, 513, 210
Shields, J. C. 2007, in ASP Conf. Ser., 373, The Central Engine of Active Galactic Nuclei, ed. L. C. Ho & J. W. Wang (San Francisco, CA: ASP), 355, arXiv:astro-ph/0612613
Shin, J., Nagao, T., Woo, J.-H., & Le, H. A. N. 2019, ApJ, 874, 22
Shin, J., Woo, J.-H., Nagao, T., & Kim, S. C. 2013, ApJ, 763, 58
Śniegowska, M., Marziani, P., Czerny, B., et al. 2021, ApJ, 910, 115
Sulentic, J. W., Marziani, P., & Dultzin-Hacyan, D. 2000, ARA&A, 38, 521
Taylor, M. B. 2005, in ASP Conf. Ser., 347, Astronomical Data Analysis Software and Systems XIV, ed. P. Shopbell, M. Britton, & R. Ebert (San Francisco, CA: ASP), 29
Terlevich, E., Díaz, A. I., & Terlevich, R. 1990, RMxAA, 21, 218
Tripathi, S., McGrath, K. M., Gallo, L. C., et al. 2020, MNRAS, 499, 1266
Vanden Berk, D. E., Richards, G. T., Bauer, A., et al. 2001, AJ, 122, 549
Verner, E., Bruhweiler, F., Johansson, S., & Peterson, B. 2009, PhST, 134, 014006
Verner, E. M., Verner, D. A., Korista, K. T., et al. 1999, ApJS, 120, 101
Veron-Cetty, M. P., & Veron, P. 2010, A&A, 518, A10
Vestergaard, M., & Wilkes, B. J. 2001, ApJS, 134, 1
Wandel, A. 1999, ApJ, 527, 657
Wang, J., Wei, J. Y., & He, X. T. 2005, A&A, 436, 417
Wildy, C., Czerny, B., & Panda, S. 2019, A&A, 632, A41
Yu, L.-M., Bian, W.-H., Wang, C., Zhao, B.-X., & Ge, X. 2019, MNRAS, 488, 1519
Zamfir, S., Sulentic, J. W., Marziani, P., & Dultzin, D. 2010, MNRAS, 403, 1759